# REPORT DOCUMENTATION PAGE

Public reporting burden for this collection of information is estimated to average 1 hour per response, including the time for reviewing instructions, searching existing data sources, gathering and maintaining the data needed, and completing and reviewing this collection of information. Send comments regarding this burden estimate or any other aspect of this collection of information, including suggestions for reducing this burden to Department of Defense, Washington Headquarters Services, Directorate for Information Operations and Reports (0704-0188), 1215 Jefferson Davis Highway, Suite 1204, Arlington, VA 22202-4302. Respondents should be aware that notwithstanding any other provision of law, no person shall be subject to any penalty for failing to comply with a collection of information if it does not display a currently valid OMB control number. **PLEASE DO NOT RETURN YOUR FORM TO THE ABOVE ADDRESS.**

| 1. REPORT DATE (DD-MM-YYYY) | 2. REPORT TYPE | 3. DATES COVERED (From - To) |
|---|---|---|
| Aug 99 | Journal Article | 1998 |

**4. TITLE AND SUBTITLE**
Zero-bias offsets in the low-temperature dark current of quantum-well infrared photodetectors

**5a. CONTRACT NUMBER**

**5b. GRANT NUMBER**

**5c. PROGRAM ELEMENT NUMBER**
62601F

**6. AUTHOR(S)**
D.A. Cardimona and Anjali Singh

**5d. PROJECT NUMBER**
4846

**5e. TASK NUMBER**
CR

**5f. WORK UNIT NUMBER**
C1

**7. PERFORMING ORGANIZATION NAME(S) AND ADDRESS(ES)**

Air Force Research Laboratory
Space Vehicles Directorate
3550 Aberdeen Ave. SE
Kirtland AFB, NM 87117-5776

**8. PERFORMING ORGANIZATION REPORT NUMBER**

**9. SPONSORING / MONITORING AGENCY NAME(S) AND ADDRESS(ES)**

**10. SPONSOR/MONITOR'S ACRONYM(S)**

**11. SPONSOR/MONITOR'S REPORT NUMBER(S)**

**12. DISTRIBUTION / AVAILABILITY STATEMENT**
Approved for Public Release; Distribution is Unlimited.

**13. SUPPLEMENTARY NOTES**
Published in Opt. Eng. 38(8) 1424-1432 (August 1999)

20050201 022

**14. ABSTRACT**

Quantum-well infrared photodetectors (QWIPs) have potential applicability in many remote-sensing applications, even in the space environment where low background fluxes are involved. In this environment, the detector arrays may need to be operated at temperatures lower then 77 K. At these temperatures, tunneling mechanisms such as Fowler-Nordheim and trap-assisted tunneling could dominate the dart current. The device resistance, which is bias-dependent, increases by several orders of magnitude at these temperatures and may pose a problem. We have seen offsets in the current-versus-voltage (I-V) characteristics (nonzero current at zero bias not associated with dopant migration) which could impair the compatibility of a QWIP array with a readout circuit. We propose that these offsets are due to an $RC$ time-constant effect. We further propose that the resistance in this time constant is due to tunneling mechanisms (and not due to contact resistance), which in turn are structure- and bias-dependent. We discuss our observations and present a circuit model of a QWIP that explains these observations nearly completely.

**15. SUBJECT TERMS**
quantum well infrated phothdetectors, zero-bias, tunneling mechanisms

| 16. SECURITY CLASSIFICATION OF: | | | 17. LIMITATION OF ABSTRACT | 18. NUMBER OF PAGES | 19a. NAME OF RESPONSIBLE PERSON |
|---|---|---|---|---|---|
| **a. REPORT** | **b. ABSTRACT** | **c. THIS PAGE** | Unlimited | 10 | Mr. David Cardimona |
| Unclassified | Unclassified | Unclassified | | | **19b. TELEPHONE NUMBER** (include area code) (505) 846-5807 |

# Zero-bias offsets in the low-temperature dark current of quantum-well infrared photodetectors

**A. Singh,** MEMBER SPIE
**D. A. Cardimona**
Air Force Research Laboratory
VSSS
3550 Aberdeen Ave. SE
Kirtland Air Force Base, New Mexico 87117

**Abstract.** Quantum-well infrared photodetectors (QWIPs) have potential applicability in many remote-sensing applications, even in the space environment where low background fluxes are involved. In this environment, the detector arrays may need to be operated at temperatures lower than 77 K. At these temperatures, tunneling mechanisms such as Fowler-Nordheim and trap-assisted tunneling could dominate the dark current. The device resistance, which is bias-dependent, increases by several orders of magnitude at these temperatures and may pose a problem. We have seen offsets in the current-versus-voltage ($I$-$V$) characteristics (nonzero current at zero bias not associated with dopant migration) which could impair the compatibility of a QWIP array with a readout circuit. We propose that these offsets are due to an $RC$ time-constant effect. We further propose that the resistance in this time constant is due to tunneling mechanisms (and not due to contact resistance), which in turn are structure- and bias-dependent. We discuss our observations and present a circuit model of a QWIP that explains these observations nearly completely. © *1999 Society of Photo-Optical Instrumentation Engineers.* [S0091-3286(99)01908-X]

## 1 Introduction

Quantum-well infrared photodetectors (QWIPs) have two major issues that impede their performance: low optical conversion efficiency and high dark current. In this paper, we will concentrate on the dark-current issues. In a QWIP detector, there are two sources of dark current: phonon- and thermally assisted emission, which dominate at higher temperatures, and trap-assisted and Fowler-Nordheim tunneling, which dominate at lower temperatures. The tunneling limit is the lowest achievable dark current of a device. Most of the dark-current reduction efforts to date have been focused in the high-photon background regime and aimed at increasing the operating temperature for detection at higher backgrounds. Hence, numerous research groups have developed several approaches to reducing the high-temperature dark current. The first QWIP structure was designed with two bound states in the well.[1] Application of a bias voltage allowed the photoexcited electrons to tunnel out of the wells and into the continuum states. The barriers in this structure were relatively narrow (<100 Å), and the bias voltage required for maximum responsivity was high (~9 V). Subsequently, a bound-to-continuum structure was proposed,[2] where the upper energy level was pushed into the continuum. Although the responsivity was reduced due to the reduction in oscillator strength, the dark current was reduced by several orders of magnitude for two reasons: a smaller bias was required for optimum responsivity, and wider barriers were permitted, thus reducing the tunneling component of the dark current. The structure that is a compromise between these two approaches and achieves both high responsivity and low dark current is the bound-to-

quasibound structure, where the second energy level is close to the continuum, but is still considered a bound state. Optimization of the well doping and barrier widths for this structure has also been performed. Other structures that have aimed at dark-current reduction are bound-to-miniband,[3,4] graded barrier,[5] and the quantum-well transistor.[6] Other types of quantum-well photodetectors, such as $p$-type strained layer superlattices[7] and bound-to-quasibound structures grown by metal-organic chemical vapor deposition (MOCVD), also show promise of low dark current at higher operating temperatures. In this paper we have chosen samples that are representative of the most common $n$-type band structures.

The environment that presents the severest constraints on dark current is space. Space-based sensors must deal with backgrounds of the order of $10^{13}$ photons/cm$^2$ s or less, requiring low-temperature operation (~40 K) in order to reduce the internal detector noise below the background noise. At these operating temperatures, the dark current in long-wavelength infrared (LWIR) QWIPs is dominated by tunneling mechanisms, and a different approach to reducing this dark current is essential. We have observed an interesting effect while studying the low-temperature dark current in QWIPs in several of the structures mentioned above.[8,9] The low-temperature current-voltage ($I$-$V$) characteristics showed a pronounced offset effect, i.e., a nonzero current at zero applied bias. The offset was found to be approximately 1 V, and to depend on a time delay in the application of the bias, indicative of an $RC$ time-constant effect. Observation of a nonzero current under zero bias in a photoconductive device has been seen by others. However, it was attributed

either to the capacitance in the cables used in the measurement setup, to poor contacts, or to dopant migration, and was considered unimportant at 77 K or higher. We have been able to rule out cable capacitance, since it would be in parallel with any device resistance, and the existence of an $RC$ time constant requires a capacitance in series with a resistance. We have also ruled out a high contact resistance as the source of the observed offset, as is shown in Sec. 2. Also, this offset effect is in addition to any offsets due to dopant migration (which would lead to a time-independent offset), and can be quite pronounced at lower temperatures. Therefore, for the low-temperature operation required of space-based sensors, this effect could be very important not only for overall device performance but also for its mating to readout electronics.

In this paper, we present an $RC$ circuit model of a QWIP to explain the time-constant effects in the low-temperature (40-K) dark current. Recently there have been several QWIP models that have included resistance and capacitance effects.[10,11] A parallel $RC$ circuit representation of a QWIP structure has been used to model a QWIP for impedance spectroscopy,[12] or to describe the nonuniform vertical charge transport and relaxation in QWIPs.[13] The significant feature of our model is the addition of a resistance in series with the capacitance. We propose that the series resistance in this $RC$ circuit is due to tunneling mechanisms (which dominate the dark current at lower temperatures), which in turn are structure- and bias-dependent. The capacitance is a *barrier capacitance* that can give rise to a quantum-mechanical separation of charge by the barriers and has been described by Ershov et al.[14] The unusual capacitance behavior of QWIPs with frequency and bias has also been observed by Ershov et al.[15] We have applied our $RC$ circuit model to several QWIP structures and found that it describes their low-temperature $I$-$V$ characteristics very well.

In the next section we describe the model to explain this offset effect associated with low-temperature dark currents in QWIP detectors. Our experimental techniques and some general observations are described in Sec. 3. Comparisons of the experimental observations with the model predictions are described in Sec. 4. Finally, the conclusions and the implications of our study are discussed in Sec. 5.

## 2 The Model

In this section we describe an $RC$ circuit model of a QWIP (see Fig. 1) to explain the $I$-$V$ offset described in Sec. 1. A QWIP detector is a photoconductor with a mesa structure. The conductivity of the detector, and hence its resistance, is governed by the doping concentration, the integrity of the contacts, the bandgap structure (bound-to-continuum versus bound-to-quasibound, etc.), and the pixel area. Capacitance within the QWIP itself contributes to the $I$-$V$ characteristics via the charge accumulation within the wells separated by the barriers. In addition, there is an external capacitance, or geometric capacitance[14] due to the geometry of the device including the contacts, which are generally made on either side of the mesa structure. Ershov et al.[16] have suggested that the potential drop across the QWIP structure is not uniform, due to the barrier potential at the emitter contact. We would like to point out that ours is a linear model, i.e., the voltage drop is taken to be equal across each circuit element.
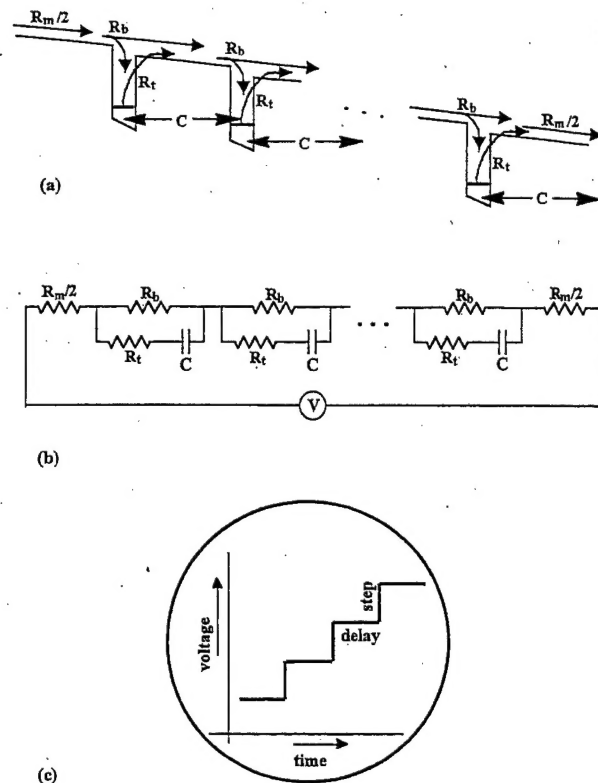


**Fig. 1** (a) Band structure of a typical QWIP showing the sources of the resistances and capacitance used in the circuit model. (b) $RC$-circuit equivalent of a QWIP. (c) Schematic of the bias versus time for the $I$-$V$ measurements.

We picture three main components to the overall low-temperature resistance of a QWIP. There is an ohmic *bulk* resistance due to electron propagation through the continuum states ($R_{\text{bulk}}$), a bias-dependent *dynamic* resistance to current passing each quantum well due to the probability of capture by the well ($R_{\text{capture}}$), and another dynamic resistance that arises from electrons attempting to escape from the quantum wells via phonon-assisted or thermally assisted excitation or via Fowler-Nordheim or trap-assisted tunneling ($R_{\text{escape}}$). In Fig. 1, we label these various resistances as $R_b = R_{\text{bulk}} + R_{\text{capture}}$ and $R_t = R_{\text{escape}}$. In the figure, we also label a mesa contact resistance ($R_m$). We have measured this resistance at room temperature and found it to be less than 100 $\Omega$. Since the contact resistance is independent of temperature, it does not affect the $I$-$V$ offset that is the subject of this paper.

The bulk resistance can be estimated very roughly as follows:

$$R_{\text{bulk}} = \frac{L}{\sigma A} = \frac{L}{en\mu A}, \qquad (1)$$

where $L$ = length, $\sigma$ = conductivity, $e$ = electronic charge, $n$ = charge density, $\mu$ = mobility, and $A$ = area. Using a mobility of around $10^3$ cm$^2$/V s (for a GaAs/AlGaAs quantum-well structure),[17] a length of 350 Å, a pixel area of (100 $\mu$m)$^2$, and a charge density given by

$$n = n_0 e^{-(E_c - E_F)/kT}, \qquad (2)$$

with $n_0 \sim 10^{18}/cm^3$, $E_c - E_F \approx 0.125$ eV (i.e., $\approx 10$-$\mu$m infrared response), and $T = 50$ K, we find the bulk resistance to be around $10^9 \Omega$. At 40 K it is of the order of $10^6 \Omega$. The resistance due to capture by the quantum wells can be thought of in terms of the probability of capture as follows:

$$R_{capture} \approx \frac{R_{bulk} p_{capture}}{1 - p_{capture}}, \qquad (3)$$

so that $R_{capture}$ becomes infinite when the probability of capture is 100%, and it is zero if the probability of capture is zero. Here, $p_{capture} = p_{phonon\,out}$ (the probability of capture via phonon emission). We therefore find for $R_b$

$$R_b \approx \frac{R_{bulk}}{1 - p_{capture}}, \qquad (4)$$

so that $R_b$ is infinite if the probability of capture is 100% and is $R_{bulk}$ if the probability of capture is zero (i.e., if the well is not there). Similarly, the leakage resistance due to escape from the quantum wells can be written as

$$R_t = R_{escape} \approx \frac{R_{bulk}}{p_{escape}}, \qquad (5)$$

so that $R_t$ is infinite when the probability for escape is zero and is $R_{bulk}$ when the probability for escape is 100% (again, if the well is not there). Here, $p_{escape} = p_{phonon\,in} + p_{thermal} + p_{tunnel}$ ($p_{phonon\,in}$ = probability of escape via phonon absorption, $p_{thermal}$ = probability of escape via thermal assistance, and $p_{tunnel}$ = probability of escape via tunneling). Thermionic emission, phonon-assisted capture and escape, and tunneling escape rates have been studied quite extensively over the past few years.[18–26]

The internal capacitance due to the quantum wells themselves can be approximated as follows:

$$C_0 = \frac{\epsilon(x) \epsilon_0 A}{d}, \qquad (6)$$

where $\epsilon(x) = 13.18 - 3.12x$, $\epsilon_0 = 8.85 \times 10^{-12}$ C$^2$/N m$^2$, $A$ = area of pixel, and $d$ = length of barrier between wells. Using $x = 0.3$ (Al mole fraction), area = $(100\,\mu m)^2$, and barrier length = 300 Å, we see that $C_0$ can be of the order of 0.4 pF. For each device, we will determine its own $C_0$ value. This calculation merely shows the order of magnitude that we can expect. The capacitance indicated in the QWIP circuit diagram is then related to this value by

$$C = (1 - p_{escape}) C_0, \qquad (7)$$

so that $C$ becomes zero when the probability of escape from the wells is 100% (i.e., when the existence of the wells is immaterial, the effect of the capacitance is nonexistent).

We first applied a circuit model in which the $R_t$ of Fig. 1 was not present (i.e., merely a capacitor and a resistor in parallel[12,13]). Since the bulk resistance is so large and the mesa resistance is only around 100 $\Omega$, this circuit led to an $RC$ time constant in which the role of the resistance was

taken solely by the mesa resistance. Therefore, the time constant for this circuit did not lead to any residual dark current when the bias was turned to zero. With a capacitance of picofarads, a resistance of the order of $10^{11} \Omega$ or greater is required in order to predict the kinds of current offsets that are seen in the experimental data. It is for this reason that we have proposed the circuit shown in Fig. 1, which includes a large quantum-well tunneling leakage resistance in series with the quantum-well capacitance. This circuit leads to the following equation for the voltage drop across the quantum-well capacitor:

$$\left( N + \frac{R_m}{R_b} + \frac{R_m}{R_t} \right) R_t C \frac{dv_c}{dt} + \left( N + \frac{R_m}{R_b} \right) v_c - V = 0, \qquad (8)$$

where $V$ is the applied bias voltage and $N$ is the number of quantum wells in the device. When the bias voltage is taken to be the stairstep function shown in Fig. 1(c), the dark current derived from this equation is

$$I = \frac{R_b + R_t}{R_m + NR_b} \frac{V_j}{R'} - \sum_{i=0}^{j} \left( \frac{R_b/R'}{1 + R_m/NR_b} \right) \frac{V_j}{R_m + NR_b}$$
$$\times (1 - e^{-\Delta t/R'C}) e^{-(t_j - t_i)/R'C} \qquad (9a)$$

$$\approx \frac{R_b + R_t}{NR_b R_t} V_j - \sum_{i=0}^{j} \frac{V_j}{NR_t} (1 - e^{-\Delta t/R_t C}) e^{-(t_j - t_i)/R_t C}, \qquad (9b)$$

where the resistance $R'$ is given by

$$R' = R_t + \frac{R_m R_b}{R_m + NR_b} \approx R_t, \qquad (10)$$

and the approximate equalities used above are good when $R_m \ll R_b$, $R_t$ (as is the case here).

From the equation for the dark current $I$, we see that the equivalent resistance for the circuit in steady state is

$$R_{eq} = NR_b + R_m. \qquad (11)$$

We take this equivalent resistance to be the dynamic resistance measured during the experiment. We also take $R_t$ to be a dynamic, voltage-dependent quantity, if not the same as $R_{eq}$, then closely related to it. Using the experimental data, we numerically take the reciprocal of the derivative of the dark current to find the bias-dependent $R_{eq}$. The maximum value of this dynamic resistance occurs at $V = 0$ and results in the maximum value for the $RC$ time constant. The minimum value of this equivalent resistance occurs when the bias voltage is maximum, and yields the maximum dark-current value.

For the theoretical fit to the experimental data, we took both $R_t$ and $R_b$ to be bias-dependent. The first is bias-dependent due to Fowler-Nordheim tunneling, and the second is bias-dependent due to the capture probability being dependent on the velocity with which the electrons drift past the quantum wells. For the bias dependence of $R_{eq}$, we tried both Gaussian and Lorentzian functions, and found

that the best fit to the curvature of both the raw current data as well as the log of the dark current occurred when we used the Lorentzian. The Lorentzian we used is

$$R_{eq} = \frac{a\gamma^2}{(V - V_0)^2 + \gamma^2} + b, \tag{12}$$

where the constants $a$ and $b$ are given by using the maximum equivalent resistance at $V_0$ and the minimum equivalent resistance at $\pm 5$ V, each calculated from the measured dark current. Here, of course, $\gamma$ represents the width of the Lorentzian function.

To summarize our numerical fitting procedure: We first measured the maximum dark current at the maximum bias to determine the minimum for the equivalent resistance in Eq. (11). Assuming $R_t$ was equal to $R_b$, we determined the maximum equivalent resistance by estimating the $RC$ time constant required to yield the experimental offset value, after approximating the capacitance $C$ from the experimentally measured device capacitance. We approximated the half-width of the Lorentzian to be used by looking at the reciprocals of the numerical derivatives of the dark-current curves at zero bias. Once all these values were determined, we slightly varied $C$, the maximum and minimum values of $R_{eq}$, the half-width of the Lorentzian bias dependence, and the proportionality factor between $R_t$ and $R_b$ until the experimental data (not only the offset value itself, but the shapes of the raw dark current and log of the dark current curves as well) were reproduced.

In order to verify if the series resistance was due to poor contacts, instead of tunneling mechanisms, we applied the above model with a high contact resistance $R_m$ (instead of the low value of 100 $\Omega$) and eliminated the tunneling resistance $R_t$. Although the offset could be reproduced, the curve shapes [raw dark current versus bias, log(dark current) versus bias, and dynamic resistance versus bias] were all very different from the experimental data.

## 3 Experimental Details

The experiment was designed to measure the resistance and capacitance of the detector. Both $I$-$V$ and capacitance measurements were performed on a select group of QWIP detectors. The dynamic resistance of the detector at low biases, the capacitance, and the $RC$ time constant were inferred from these measurements.

Precise $I$-$V$ measurements were made using a Keithley 236 Source Measure unit under computer control. The measurement involves the application of a dc bias for a specified time interval (delay) and the measurement of the dc current at the end of that interval. The resolution of this unit, specified by the manufacturer, is 10 fA. The device was mounted in a dewar cooled with liquid helium, and a darkened metal plate was placed at the aperture of the dewar. A cold shield maintained at 77 K was inserted over the device. All these precautions were taken to ensure that the current we measured was the dark current at a low background of $10^9$ photons/cm$^2$ s or less.

The $I$-$V$ characteristics of these devices were measured at 40 K, at 77 K, and at room temperature. From the room-temperature measurements, we inferred that the contact resistance ($R_m$) was less than 100 $\Omega$. While no offsets were observed at 77 K, some devices showed significant offsets ($\sim 1$ V) in the $I$-$V$ characteristics at the lower temperatures. The magnitude of the offset decreased as the delay was increased, and the sign of the offset switched polarity when the direction of the bias scan was reversed. The delay between bias turn-on and current measurement was varied from 1 s up to 60 s in order to observe the time-constant effects. The bias was scanned from $+5$ to $-5$ V and vice-versa.

Capacitance measurements were also made on these devices using a SULA Technologies capacitance meter. The capacitance was measured at several temperatures, including 40 and 77 K. The capacitance showed sharp temperature dependence, starting at a significant value at the low temperatures and becoming negligible at 77 K. The capacitance was measured at a standard frequency of 1 MHz. At this frequency, the capacitance is fairly bias-independent.

The devices chosen for this study are representative of many QWIP detectors that have been developed to date. The effect of the structure, doping concentration, and pixel size on the magnitude of the offsets was investigated. Devices used in this study were obtained from the Industrial Microelectronics Center in Sweden, AT&T, and Lockheed-Martin.

## 4 Comparison with the Model

In this section, we compare our experimental and theoretical results for the four devices (devices A through D) used in this study. For each of these devices, we first give a representation of their band structures. Then we show the experimental and theoretical curves for log(dark current) versus bias in order to present the offset information, raw dark current versus bias to indicate the theoretical and experimental matching of curve shapes, and the dynamic equivalent resistance calculated from both the experimental and theoretical dark-current curves. Note that all of the data we present here is for 40 K, since none of the devices showed an offset at 77 K.

The first devices we investigated (devices A and B) were bound-to-quasibound (BQB) structures from the Industrial Microelectronics Center (IMC) of Sweden. The two devices had different doping concentrations, but the common band structure for each is represented in Fig. 2(a). Also common to both of these devices was the fact that a bonding pad composed of the same quantum-well structure as the devices themselves was used. This resulted in a series of $N$ quantum wells within each device, in parallel with another series of $N$ quantum wells within the bonding pad. This setup leads to a device capacitance given by the following:

$$C_{measured} = C_{device} + C_{pad} \tag{13a}$$

$$= \frac{\epsilon(x)\epsilon_0(A_{device} + A_{pad})}{Nd} \tag{13b}$$

$$\Rightarrow C_{device} = C_{measured}\frac{A_{device}}{A_{device} + A_{pad}}. \tag{13c}$$

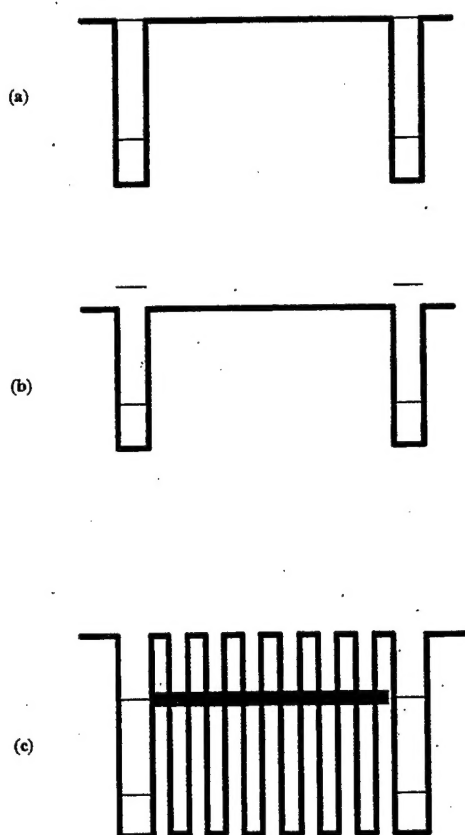Using this $C_{device}$, we find the $C_0$ of each quantum well for the circuit analysis as

**Fig. 2** Band diagram of (a) a bound-to-quasibound structure, (b) a bound-to-continuum structure, and (c) a bound-to-miniband structure.

$$C_0 = N C_{device} . \tag{14}$$

The bonding pads for each of these first two devices were 200-$\mu$m squares. With an external capacitance of only 1 pF, with each device being composed of 50 quantum wells, and with device areas that were 150 $\mu$m square for device A and 100 $\mu$m square for device B, the measured capacitances of 77 and 38 pF lead to quantum-well capacitances of $1.4 \times 10^{-9}$ and $0.4 \times 10^{-9}$ F for devices A and B, respectively.

Figures 3 and 4 show the experimental and theoretical results for these devices. In general, we see that these BQB structures have very narrow Lorentzian dynamic resistances, with very large peak values. The narrow widths of these Lorentzians result in a relatively narrow region of flattening of the current-versus-bias curves near zero bias. The large peak resistances result in large offsets (i.e., large $RC$ time constants, leading to longer time delays before steady state is reached). Device A had a larger doping concentration than device B, resulting in a peak resistance for device A less than that for device B (approximately $1.4 \times 10^{13}$ versus $5 \times 10^{13}$ $\Omega$), and hence an $RC$ time constant and an offset that were smaller for device A than for device B. Notice that both the experimental data and the theoretical model show a pronounced asymmetry at $V=0$ in the log(dark current)-versus-bias curve for device B. The final numerical fit parameters used to reproduce the experimental data for each device are listed in the captions for Figs. 3

and 4. We would like to point out that this effect is not unique to these MOCVD-grown devices from IMC, Sweden. Offsets of similar magnitude have been observed in all other BQB devices we have subsequently characterized.

Device C is a bound-to-continuum (BC) structure from AT&T and shown schematically in Fig. 2(b). This device did not have an additional bonding pad; wires were taken directly from the device itself. Therefore, in Eq. (13) we set $A_{pad}=0$. With this device having 34 quantum wells and a measured capacitance of 10 pF, Eq. (14) results in a quantum-well capacitance of about $3.4 \times 10^{-9}$ F. The experimental and modeled data are shown in Fig. 5. Note that this BC structure has a broader Lorentzian lineshape for the equivalent resistance than the BQB structures from the IMC had. This is the reason there is a broader area of flatness in the current-versus-bias curves. In addition, the peak value of this resistance (approximately $4 \times 10^{10}$ $\Omega$) is much smaller, as expected, since the ground state is much shallower within the well for BC-type structures, and hence the escape probability is greater. This two-order-of-magnitude-smaller resistance leads to an $RC$ time constant that is much smaller than for the BQB structures, and thus to a steady state that is reached much sooner. This results in there being no offset in the dark current for this BC structure. Further, note that the asymmetries in the dark current and the log(dark current) curves are reproduced very well by the model. The final model parameters are again listed in the figure caption. In this case, to better match the experimentally determined dynamic resistance function, we used Lorentzian sides connected by a linearly increasing function to model the dynamic resistance in this case.

Device D is a bound-to-miniband (BM) structure from Lockheed Martin, shown in Fig. 2(c). This device also did not have the separate bonding pad, and so $A_{pad}=0$. With device D having 40 quantum wells and a measured capacitance of 70 pF, the quantum-well capacitance is approximately $2.4 \times 10^{-9}$ F. The experimental and numerical data are plotted in Fig. 6, with the model parameters given in the caption. The equivalent resistance is very broad and nearly bias-independent, leading to a nice linear current-versus-bias curve. The maximum resistance value (approximately $1.4 \times 10^{11}$ $\Omega$) was greater than for the BC structure and less than for the BQB structure, because a BM structure has two possibilities for tunneling: into the miniband and into the continuum. Although it is easier to tunnel into the miniband than into the continuum, the resistance of the miniband is greater than that of the continuum. Once again, we see that the device had a small enough resistance that no offset was present. Finally, we see that the nearly perfect symmetry of this device is, once again, reproduced very nicely by the model.

## 5 Conclusions and Implications

In this study, we have attempted to explain the presence of a large nonzero dark current when the applied bias voltage is zero. We call this effect an *offset* in the $I$-$V$ characteristics and recognize that this is in addition to any intrinsic biasing present due to dopant migration. This offset effect is observed only at low temperatures ($<50$ K), when the dark currents are very low. We have proposed an $RC$ circuit model that includes a bias-dependent (''dynamic'') tunnel-
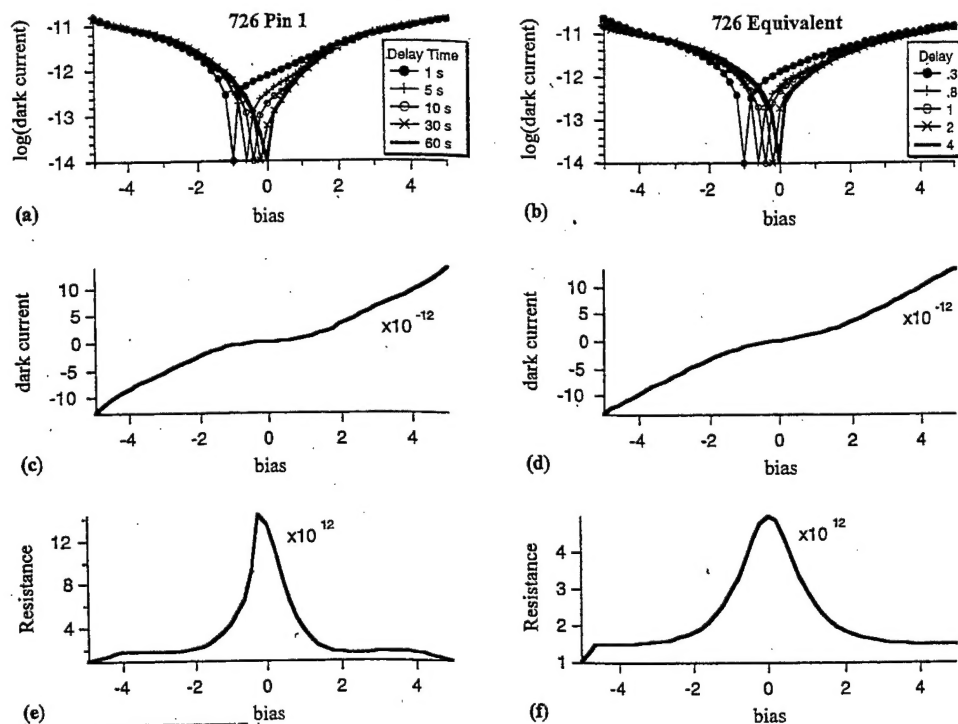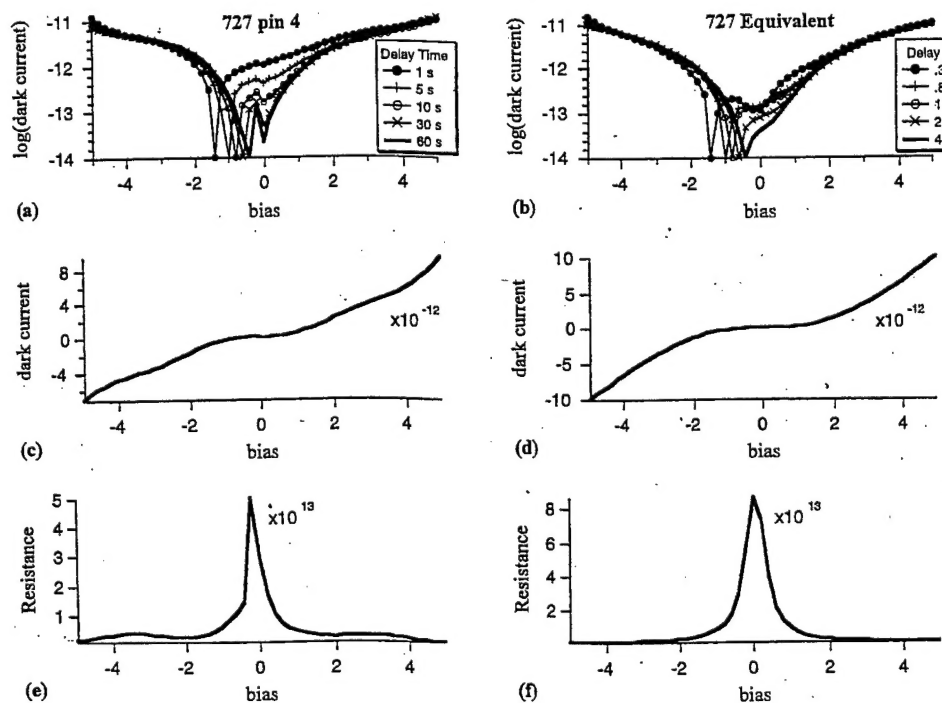
**Fig. 3** Experimentally measured [(a), (c), and (e)] and theoretically calculated [(b), (d), and (f)] $I$-$V$ characteristics for the IMC device with high doping (device A). (a) and (b) show the log of the absolute value of the dark current (A) for various time delays. In (b) $R_{eqmax}=1\times10^{12}\,\Omega$, $R_{eqmin}=3.8\times10^{11}\,\Omega$, $C=1.4\times10^{-10}$ F, $\gamma=1.5$, and $R_t=R_b$. (c) and (d) show the dark current (A), and (e) and (f) show the resistance ($\Omega$) (calculated as the reciprocal of the derivative of the dark-current curves) as functions of bias (V).



**Fig. 4** Experimentally measured [(a), (c), and (e)] and theoretically calculated [(b), (d), and (f)] $I$-$V$ characteristics for the IMC device with low doping (device B). (a) and (b) show the log of the absolute value of the dark current for various time delays. In (b) $R_{eqmax}=2\times10^{13}\,\Omega$, $R_{eqmin}=5\times10^{11}\,\Omega$, $\gamma=0.5$, $C=4.8\times10^{-11}$ F, and $R_t=R_b$ except that $R_{tmax}=0.5R_{bmax}$. (c) and (d) show the dark current (A), and (e) and (f) show the resistance ($\Omega$) (calculated as the reciprocal of the derivative of the dark-current curves) as functions of bias (V).
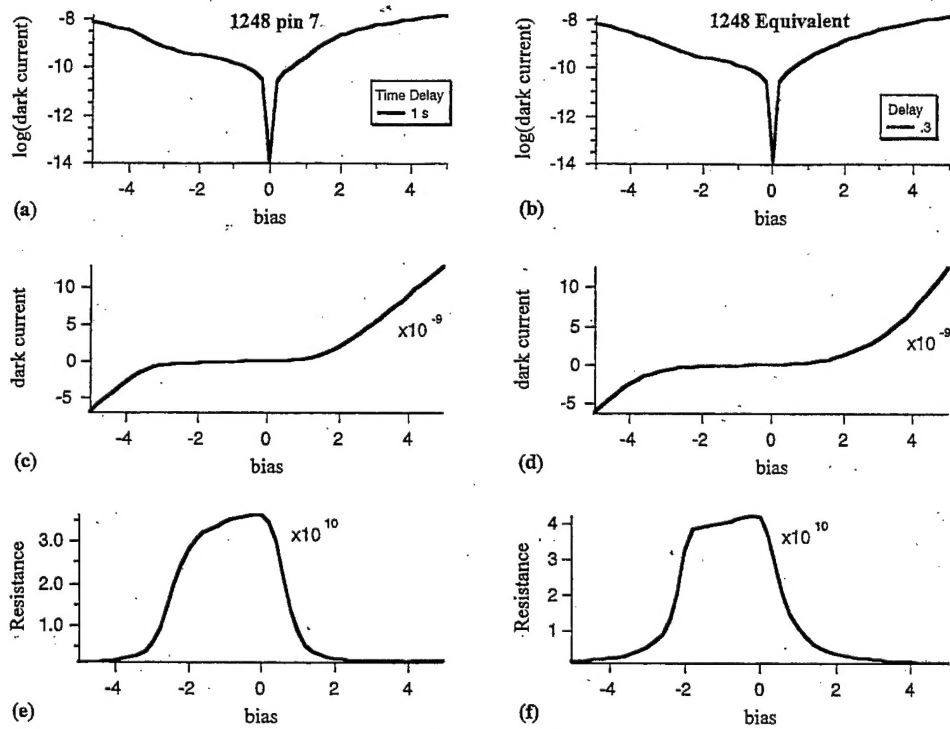
**Fig. 5** Experimentally measured [(a), (c), and (e)] and theoretically calculated [(b), (d), and (f)] $I$-$V$ characteristics for the AT&T device (device C). (a) and (b) show the log of the absolute value of the dark current (A) for various time delays. In (b) $R_{eqmax}$=8.0 and $8.5\times10^9$ $\Omega$ at $-2$ V and at 0 V, $R_{eqmin}$=8.0 and $4.0\times10^8$ $\Omega$ at $-5$ V and at $+5$ V, $\gamma_{left}$=1.0=$\gamma_{right}$, $C$=$3.4\times10^{-11}$ F, and $R_t$=$R_b$. (c) and (d) show the dark current (A) and (e) and (f) show the resistance ($\Omega$) (calculated as the reciprocal of the derivative of the dark-current curves) as functions of bias (V).
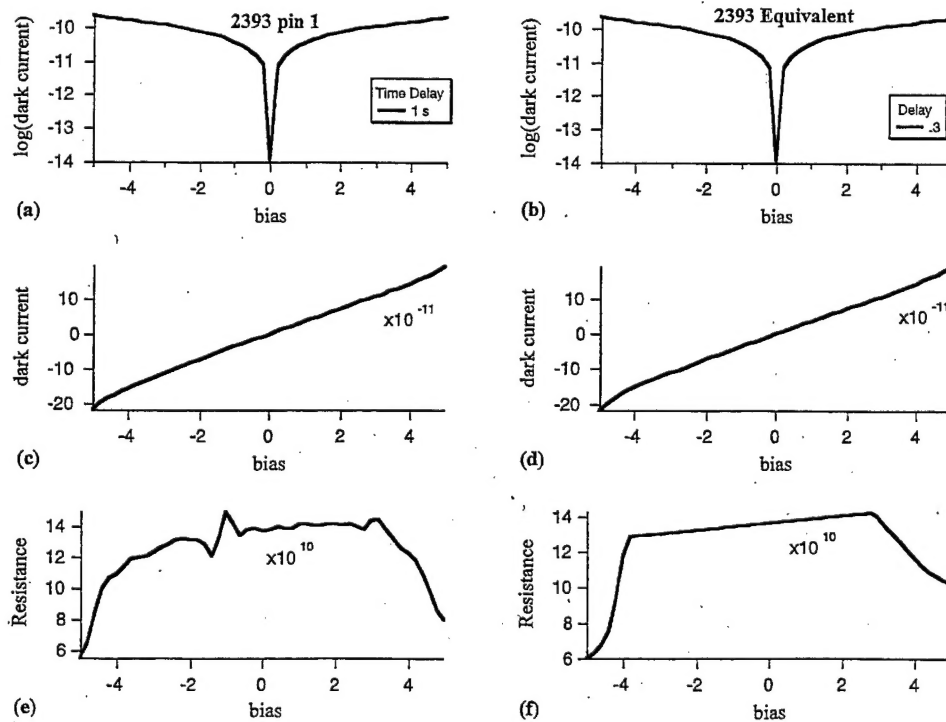
**Fig. 6** Experimentally measured [(a), (c), and (e)] and theoretically calculated [(b), (d), and (f)] $I$-$V$ characteristics for the Lockheed Martin device (device D). (a) and (b) show the log of the absolute value of the dark current (A) for various time delays. In (b) $R_{eqmax}$=2.65 and $2.8\times10^{10}$ $\Omega$ at $-4$ V and at $+3$ V, $R_{eqmin}$=2.3 and $2.6\times10^{10}$ $\Omega$ at $-5$ V and at $+5$ V, $\gamma_{left}$=1.0, $\gamma_{right}$=3.0, $C$=$1\times10^{-10}$ F, and $R_t$=$R_b$. (c) and (d) show the dark current (A), and (e) and (f) show the resistance ($\Omega$) (calculated as the reciprocal of the derivative of the dark-current curves) as functions of bias (V).

ing ("leakage") resistance in series with a quantum-well capacitance in addition to the usual bulk resistance in parallel with the well capacitance. We found that it is the presence of this leakage resistance in series with the well capacitance that produces an $RC$ time constant that, in turn, results in the observed current offsets. Using this circuit model, we derived an equation for the dark current that provides an excellent fit to the experimental data. With a Lorentzian shape for the bias dependence of the tunneling resistance, we were able to reproduce both the offset itself as well as the asymmetries in the curve shapes. This model is, of course, very preliminary; however, it must contain much of the physics of the processes involved for the data to fit so well. The absence of the offset at higher temperatures is also predicted by this model, since the resistance and capacitance have strong inverse temperature dependence and are several orders of magnitude smaller at 77 K.

Because the tunneling resistance was of the utmost importance for describing the offset effect, it is obvious that both the QWIP band structure and doping concentration will be very important. Quantum-well capacitance is also an important factor, but in the present study all of the capacitances for each of the devices were very similar and therefore played only a minor role. Further, because the offset effect is due to an $RC$ product, the pixel size or the barrier thickness will not play much of a role, since the two parameters cancel each other out. We have described both the series tunneling resistance and the parallel bulk-related resistance, in terms of escape and capture probabilities. The bound-to-quasibound (BQB) structure has a greater tunneling resistance than either a bound-to-continuum (BC) or a bound-to-miniband (BM) structure, and therefore has the greatest offset value. The BC structure has the smallest tunneling resistance. We also found that the dynamic resistance for the BQB structure was a very narrow Lorentzian, while that of the BC structure was broader, and that of the BM was the broadest (very nearly bias-independent).

It is obvious now that the design of a QWIP structure for strategic applications, where operating temperatures must be kept below 50 K due to the low backgrounds, must include careful attention to the resistance and capacitance of the device. We do need the overall device resistance to be high in order to reduce the dark current. However, a high resistance in series with the capacitance contributes to an $RC$ time-constant effect. For extremely low backgrounds, capacitive transimpedance amplifier (CTIA) readouts (with built-in gain) are desirable. A device capacitance greater than 1 pF would make compatibility with this type of readout design difficult.

A microscopic theory of the origins of the series resistance and capacitance due to the quantum wells separated by barriers is presently under investigation in our group.

## References

1. B. F. Levine, K. K. Choi, C. G. Bethea, J. Walker, and R. J. Malik, "New 10 $\mu$m infrared detector using intersubband absorption in resonant tunneling GaAlAs superlattices," *Appl. Phys. Lett.* **50**, 1092 (1987).
2. B. F. Levine, C. G. Bethea, G. Hasnain, V. O. Shen, E. Pelve, R. R. Abbot, and S. J. Hsieh, "High sensitivity low dark current 10 $\mu$m GaAs quantum well infrared photodetectors," *Appl. Phys. Lett.* **56**(9), 851 (1990).
3. L. S. Yu and S. S. Li, "A metal grating coupled bound-to-miniband transition GaAs multiquantum well/superlattice infrared detector," *Appl. Phys. Lett.* **59**, 1332 (1991).
4. T. S. Faska, J. Little, W. Beck, K. Ritter, and A. Goldberg, "128 ×128 LWIR imaging using mini-band transport GaAs/AlGaAs multiple quantum well detectors," in *Innovative Long Wavelength Infrared Detector Workshop*, Jet Propulstion Labs (1992).
5. R. C. Lacoe, M. J. O'Loughlin, D. A. Gutierrez, W. L. Bloss, R. C. Cole, and N. Isaac, "Quantum well infrared photodetector research at the Aerospace Corporation," in *Innovative Long Wavelength Infrared Detector Workshop* (1992).
6. K. K. Choi, M. Dutta, P. G. Newman, and M. L. Saunders, "10 $\mu$m hot-electron transistors," *Appl. Phys. Lett.* **57**(13), 1348 (1990).
7. Y. H. Wang, S. S. Li, and J. Chu, "Ultralow dark current $p$-type strained layer InGaAs/InAlAs quantum well infrared photodetector with background limited performance for $T \leqslant 100$ K," *Appl. Phys. Lett.* **64**(6), 727 (1994).
8. A. Singh and D. A Cardimona, "Design issues relating to low-temperature dark current in quantum well infrared detectors," *Photodetectors: Materials and Devices II, Proc. SPIE* **2999**, 46–54 (1997).
9. A. Singh and D. A. Cardimona, "Quantum well infrared detector research at the Air Force Research Laboratory," in *Proc. 5th International Symp. on Long Wavelength Infrared Detectors and Arrays*, Electrochemical Society, Paris (1997).
10. M. Ershov, C. Hamaguchi, and V. Ryzhii, "Device physics and modeling of multiple quantum well infrared photodetectors," *Jpn. J. Appl. Phys., Part 1* **35**, No 2B, 1395–1400 (1996).
11. V. Ryzhii, "Characteristics of quantum well infrared photodetectors," *J. Appl. Phys.* **81**(9), 6442–6448 (1997).
12. F. Luc, E. Rosencher, and B. Vinter, "Determination of electron recombination parameters in GaAs/AlGaAs quantum wells by impedance spectroscopy," *Appl. Phys. Lett.* **62**, 1143 (1993).
13. A. G. U. Perera, V. G. Silveshov, S. G. Matsik, H. C. Liu, M. Buchanan, Z. R. Wasilewski, and M. Ershov, "Nonuniform vertical charge transport and relaxation in quantum well infrared detectors," *J. Appl. Phys.* **83**(2), 991–997 (1998).
14. M. Ershov, V. Ryzhii, and K. Saito, "Capacitance-voltage characteristics of multiple-quantum-well semiconductor heterostructures," *J. Phys. D* **28**, 2118–2122 (1995).
15. M. Ershov, H. C. Liu, L. Li, M. Buchanan, Z. R. Wasilewski, and V. Ryzhii, "Unusual capacitance behavior of quantum well infrared photodetectors," *Appl. Phys. Lett.* **70**(14), 1828–1830 (1997).
16. M. Ershov, V. Ryzhii, and C. Hamaguchi, "Contact and distributed effects in quantum well infrared photodetectors," *Appl. Phys. Lett.* **67**(21), 3147–3149 (1995).
17. S. Adachi, Ed., *Properties of Aluminum Gallium Arsenide*, p. 177, INSPEC, IEEE, London (1993).
18. H. Schneider and K. von Klitzing, "Thermionic emission and Gaussian transport of holes in a GaAs/AlGaAs multiple-quantum-well structure," *Phys. Rev. B* **38**, 6160 (1988).
19. M. G. Shorthose, J. F. Ryan, and A. Moseley, "Phonon-assisted tunneling of photoexcited carriers from InGaAs Quantum wells in applied electric fields," *Solid-State Electron.* **32**, 1449 (1989).
20. J. Feldman, K. W. Goossen, D. A. B. Miller, A. M. Fox, J. E. Cunningham, and W. Y. Jan, "Fast escape of photocreated carriers out of shallow quantum wells," *Appl. Phys. Lett.* **59**, 66 (1991).
21. D. J. Moss, T. Ido, and H. Sano, "Calculation of photogenerated carrier escape rates from GaAs/AlGaAs quantum wells," *IEEE J. Quantum Electron.* **30**, 1015 (1994).
22. A. Hernandez-Cabrera, P. Aceituno, and H. Cruz, "Electron-phonon interaction and tunneling escape process in GaAs/AlAs quantum wells," *J. Appl. Phys.* **78**, 6147 (1995).
23. K. R. Lefebvre and A. F. M. Anwar, "Electron and hole escape times in single quantum wells," *J. Appl. Phys.* **80**, 3595 (1996).
24. K. R. Lefebvre and A. F. M. Anwar, "Electron escape time from single quantum wells," *IEEE J. Quantum Electron.* **33**, 187 (1997).
25. Y. Zheng, T. Lu, J. Liu, and W. Su, "The effect of electron effective mass mismatch on the electron–optical-phonon scattering rate in a quantum well structure," *Semicond. Sci. Technol.* **12**, 1235 (1997).
26. A. F. M. Anwar and K. R. Lefebvre, "Electron escape via polar optical-phonon interaction and tunneling from biased quantum wells," *Phys. Rev. B* **57**, 4584 (1998).

**A. Singh** received a BE (Hons) degree from the University of Madras, India, an MS from the Indian Institute of Technology, Madras, India, and a PhD from the University of Rhode Island, all in electrical engineering. She was a National Research Council Post-Doctoral Fellow at the Air Force Phillips Laboratory, where she initially began investigating the low-temperature physics of quantum-well infrared photodetector in her laboratory. She is currently a research assistant professor at the University of New Mexico and an IPA at the Air Force Research Laboratory, where she continues to pursue her work in low-background, low-temperature quantum-well infrared photodetectors, long-wave and multicolor infrared detectors, and smart sensors.

**D. A. Cardimona** received his BS degree in physics and mathematics from Marquett University in Milwaukee, Wi, and his PhD in optics from the Institute of Optics, the University of Rochester, Rochester, NY. As a theoretical research physicist at the Air Force Research Laboratory in Albuquerque, NM, Dr. Cardimona has pursued research in quantum optics, nonlinear optics, physical optics, laser physics, quantum electronics, and quantum-well physics. He is the Component Research Group leader in the Space Sensing and Vehicle Control Branch of the Surveillance and Control Division of the Space Vehicles Directorate, and is presently investigating quantum interference effects in quantum-well semiconductor structures and dark-current mechanisms at low temperatures in quantum-well detectors.